

Low-cost yet High-Performant Sparse Matrix-Matrix Multiplication on Arm SME Architectures

Kelun Lei[★], Hailong Yang[★], Kaige Zhang[★], Kejie Ma[★], Yiqing Wang[★], Xin You[★], Yufan Xu[†], Enrique S. Quintana-Ortí[‡], Zhongzhi Luan[★], Yi Liu[★] and Depei Qian[★]

[★]Beihang University, Beijing, China [†]Independent Researcher, Cupertino, USA, [‡]Universitat Politècnica de València

{kelunlei,hailong.yang,kaige.zhang,kejiema,YiqingWang,youxin2015,07680,yi.liu,depeiq}@buaa.edu.cn
sz.yufanxu@gmail.com,quintana@uji.es

Abstract

Sparse matrix–dense matrix multiplication (SpMM) is a critical kernel in both scientific computing and emerging graph learning workloads. The recent Armv9 architecture introduces Scalable Matrix Extension (SME), enabling tile-based matrix operations with high throughput. However, effectively exploiting both SME and traditional SIMD resources for unstructured sparse workloads remains an open challenge. To address this, we propose LOOPS, a hybrid execution framework that combines row-wise CSR-part with vector-wise BCSR-part layout, enabling cooperative utilization of vector instructions (NEON) and Scalable Matrix Extension (SME) resources. LOOPS supports multi-precision SpMM across FP64, FP32, and FP16 via an adaptive two-level parallelization scheme guided by a lightweight performance model. Experimental results on the entire SuiteSparse on an Apple’s M4Pro CPU show that LOOPS achieves average speedups of 9.93 \times (FP32)/14.4 \times (FP64) against the CPU baseline TACO and 71.3 \times (FP32)/54.8 \times (FP64) with respect to Armadillo. A comparison of LOOPS running on the same CPU with two GPU methods (cuSPARSE, Magicube) executed on an NVIDIA A100 GPU show average speedups for LOOPS between 19.8 \times and 33.5 \times , depending on the precision. Notably, LOOPS delivers significantly better energy efficiency than the GPU codes on the A100 GPU.

1 Introduction

As the demand for extreme performance in traditional scientific computing and emerging deep learning applications continues to grow, many hardware vendors have introduced new architectures and instruction sets to accelerate matrix operations. Notably, recent high-end CPUs (e.g., Apple M4) incorporate outer-product matrix units, such as Armv9’s Scalable Matrix Extension (SME) [3, 5], improving both the efficiency and performance of matrix operations. However, while dense matrix operations can efficiently and conveniently leverage such matrix units for acceleration, sparse matrix operations face significant challenges in achieving optimal hardware peak performance. Among sparse matrix operations, Sparse Matrix-Matrix Multiplication (SpMM) has garnered substantial attention for its potential to reduce memory requirements and computation time in various domains, including

scientific computing [2, 7, 29], solvers [1, 28], graph neural networks (GNNs) [26, 43], and deep learning [11, 14, 32]. Therefore, investigating how to optimize SpMM to harness matrix units and improve performance on CPUs is of critical importance.

Existing CPU-side SpMM efforts [16, 23, 39, 40, 49] largely focus on vector instruction sets (e.g. NEON and AVX). In addition, code-generation-based sparse compilers [6, 9, 13, 27] and vendor or third-party libraries [4, 41, 44] also contribute to this space. Therefore, SME-style outer-product matrix units in modern CPUs still remain underutilized in sparse workloads. In contrast, GPUs with inner-product matrix units (a.k.a, Tensor Core Units, TCUs) have achieved remarkable performance on SpMM tasks. Many works [10, 15, 30, 37, 46–48] have exploited TCUs to accelerate SpMM with specialized block-based sparse formats and computation strategies. Their core optimizations include efficient data movement, overlapping memory loads and computations, pipeline-based decoupling of execution stages, and asynchronous execution. Some studies [8, 35] further explore sparse TCUs for structured sparsity patterns.

However, the above CPU/GPU techniques are not directly applicable to SME-based architectures due to three unique challenges:

- **C1: Lack of sparse-specific SME mappings.** SME units are primarily designed for dense GEMM (general matrix-matrix multiplication) kernels and no existing CPU work has established an efficient sparse storage scheme and computation dataflow for it. Inspired by GPU block-based strategies for TCUs, a natural idea is to apply similar blocking for SME. However, the zero-propagation effect in outer-product computation amplifies the cost of padding zeros within sparse blocks, causing severe waste of compute and memory bandwidth.
- **C2: Underexplored multi-precision sparse acceleration.** SME natively supports computations in FP64, FP32 and FP16 formats, but existing CPU-side SpMM frameworks seldom optimize for FP16 due to lack of hardware support. As a result, the opportunity to exploit SME for high-performance half-precision sparse computation remains largely unexplored.
- **C3: Balancing vector and matrix unit utilization.** Architectures such as Apple’s M4 series integrate both vector

(NEON) and matrix (SME) units, with SME units shared across multiple cores. Our measurements show that assigning all threads exclusively to SME execution often degrades performance for light or irregular workloads due to severe inter-core contention for SME resources, while leaving NEON pipelines underutilized. Since SME instructions execute on a dedicated pipeline distinct from vector instructions, a coordinated strategy that leverages both pipelines can maximize hardware resource utilization.

To address these challenges, we present LOOPS, a lightweight and flexible SpMM framework for CPUs with outer-product matrix units. LOOPS adopts a hybrid sparse format combining a CSR-part processed by vector instructions (e.g., NEON), and the vector-wise BCSR part, executed via matrix instructions (e.g., SME). This hybrid design mitigates padding overhead (C1), supports multi-precision SpMM including FP16 (C2), and enables cooperative utilization of vector and matrix units to avoid resource contention (C3). At runtime, LOOPS adopts a two-level parallel execution model. At the coarse level, the CSR and BCSR kernels are assigned to disjoint thread groups, enabling inter-kernel parallelism. Within each kernel, fine-grained thread parallelism with a customized implementation is applied to further accelerate computation. A lightweight quadratic performance model, calibrated via representative warm-up runs, predicts the optimal workload partition and thread allocation for a given matrix.

Our evaluation on the entire Suitesparse demonstrates that the LOOPS SpMM implementation delivers significant performance improvements over widely used sparse libraries and compilers. On the Apple M4Pro (12-core) CPU, LOOPS achieves an average speedup of 9.93 \times over TACO [27] and 71.3 \times over Armadillo [41] in FP64 precision. For FP32 precision, LOOPS provides 14.44 \times and 54.57 \times average speedups over TACO and Armadillo, respectively. For FP16 precision, we compare our method against vendor-provided and manually-optimized GPU baselines. On average, LOOPS running on the Apple M4Pro chip outperforms cuSPARSE [35] and Magicube [30] executed on an NVIDIA A100 GPU by 33.49 \times and 19.79 \times , respectively. Despite the A100 delivering high throughput in some cases, its power consumption is significantly greater. We observe that LOOPS achieves comparable or superior energy efficiency across various representative matrices. For instance, as detailed in Table 3, even when the GPU code executes faster on the A100 GPU, LOOPS' energy efficiency is still up to 20 \times higher.

The primary contributions of this paper are as follows:

- We propose LOOPS, a novel hybrid format that partitions the workload between vector and matrix units, mitigating the zero-propagation effect of outer-product computation while preserving data locality.

- We are the first to exploit SME's native FP64/FP32/FP16 support for SpMM, enabling high-performance sparse computation among different precisions on CPUs without specialized accelerators.
- We propose a hardware-aware scheduling strategy with a lightweight performance model that dynamically balances execution between vector and matrix pipelines, alleviating inter-core SME contention and maximizing throughput.
- Evaluations on SuiteSparse show LOOPS outperforms all the CPU baselines on M4Pro chip and achieves comparable performance and better energy efficiency against GPU baselines on A100 across FP64, FP32, and FP16 precisions, which demonstrates the effectiveness of the proposed framework and optimizations.

2 Background

2.1 SpMM

SpMM refers to the multiplication of a sparse matrix A with a dense matrix B , producing a dense output matrix C . There are two prominent approaches to compute SpMM: inner-product based and outer-product based methods.

Inner-Product based SpMM: This approach computes each element c_{ij} in the output matrix C as the dot (inner) product of the i -th row of A and the j -th column of B as $c_{ij} = \sum_k a_{ik} \cdot b_{kj}$, where a_{ik} and b_{kj} are non-zero elements from A and B , respectively. This method iterates over rows of A and columns of B , requiring efficient sparse row traversal and indirect memory accesses to B . While this approach aligns well with the row-major storage of sparse matrices (e.g., CSR format), its efficiency is often constrained by irregular memory access patterns and limited opportunities to leverage data reuse in B .

Outer-Product based SpMM: This alternative computes C by iterating over the non-zero elements of A and accumulating rank-1 updates as $C = \sum_k a_{:,k} \cdot b_{k,:}$, where $a_{:,k}$ is the sparse k -th column of A , and $b_{k,:}$ is the dense k -th row of B . This method emphasizes column-wise sparsity and allows for better data reuse of $b_{k,:}$. Moreover, it is naturally suited to hardware accelerators equipped with outer-product matrix units, as each rank-1 update can be mapped to efficient outer-product computations. However, the outer-product method requires carefully orchestrated memory and compute strategies to avoid excessive intermediate data accumulation and maintain computational efficiency.

2.2 Modern multi-Core CPUs and matrix extension

The advanced Armv9 architecture introduces Scalable Matrix Extension (SME) which enables innovation and acceleration across GEMM-like workloads, including those arising in AI (artificial intelligence) and machine learning applications.

Table 1. Peak performance comparison (TFLOPS for floating point, TOPS for INT8) of Apple M4Pro (12-core CPU) and NVIDIA A100 (with Tensor Cores).

Device	Precision (TFLOPS/TOPS)			
	FP64	FP32 / TF32	FP16	INT8
Apple M4Pro	1.0	4.1 (FP32)	8.3	33.3
NVIDIA A100	19.5	156 (TF32)	312	624

Although the theoretical peak performance of GPU typically surpasses that of SME-equipped CPUs as shown in Table 1, the gap can narrow significantly under real-world constraints such as memory bandwidth, workload sparsity, and power consumption. Consider the Apple M4Pro CPU, for example. Compared to high-end professional GPUs, the M4Pro chip offers several compelling advantages. First, the M4Pro demonstrates substantially lower power consumption, which not only reduces operational costs but also alleviates thermal design constraints. Specifically, the Thermal Design Power (TDP) of M4Pro is 40W which is significantly lower than 250W of A100. Despite its lower power envelope, the M4Pro achieves attainable computational performance, particularly in low-precision arithmetic operations (e.g., INT8 or FP16), where it exhibits a high throughput. This combination of low cost, energy efficiency, and strong low-precision performance results in a markedly higher performance-per-watt ratio compared to traditional GPUs, making the M4Pro an efficient and scalable solution for edge computing and AI inference workloads.

3 Methodology

3.1 Overview

Figure 1 presents an overview of our method. First, to address **C1**, LOOPS employs a hybrid format that partitions the sparse matrix into a CSR-part and a BCSR-part in a row splitting way. The BCSR-part is carefully structured to align with SME’s outer-product model without excessive padding. To determine three key parameters (**C3**), namely 1) the row boundary r_{boundary} that separates the CSR and BCSR regions, 2) the number of threads t_{neon} assigned to execute the SpMM of the CSR part, and 3) the number of threads t_{sme} for the BCSR part, we first fit a performance model using a representative set of parameter configurations to predict the optimal thread setup. Then, the row boundary r_{boundary} serves as a balancing factor that equalizes the workload and computational capability between the NEON and SME units. This parameter is set by solving the following equation

$$r_{\text{boundary}} \cdot \text{TP}_{\text{neon}} \cdot t_{\text{neon}} = (r_{\text{total}} - r_{\text{boundary}}) \cdot \text{TP}_{\text{sme}} \cdot t_{\text{sme}}, \quad (1)$$

where r_{total} is the total number of rows, while TP_{neon} and TP_{sme} specify the throughput of two processing units. Finally, the matrix is passed to the execution stage, where our

custom high-performance kernel performs the matrix multiplication. To resolve **C2**, LOOPS provides dedicated support for FP64, FP32 and FP16. In particular, our FP16 BCSR-part kernel exploits SME’s 2-way fmopa instructions, enabling high-performance mixed-precision execution.

3.2 The LOOPS format

3.2.1 Data layout representation. On architectures where multiple cores share SME units, resource contention among the threads can degrade performance. To address this, we propose a hybrid sparse format, LOOPS, which combines a row-wise CSR-part layout with a vector-wise BCSR-part layout to leverage the benefits of both NEON and SME hardware resources. This hybrid strategy allows one portion of the matrix to be handled efficiently with NEON vector instructions due to the row-aligned memory layout of CSR part. Meanwhile, the other portion benefits from SME’s matrix-level parallelism through block outer-products on structured BCSR blocks. The block mapping also enables spatial reuse, making it highly cache- and compute-efficient.

While block formats such as BCSR offer high throughput under regular sparsity patterns, they introduce significant overhead for highly sparse matrices due to the increased number of padding zeros within blocks as well as severe useless computations. Instead of using 2D tiles, LOOPS employs an asymmetric tile shape of $\text{vector_size} \times 1$. This design is compatible with the outer-product computation model of SME, in which each compute unit operates on a column tile from the sparse matrix A and the corresponding row tile from the dense matrix B . The use of this narrow tile shape reduces padding overhead and allows the tile to be used directly as input to the SME outer-product unit, leading to improved performance and resource efficiency.

3.2.2 Conversion from CSR to LOOPS. The transformation from a conventional CSR format to our LOOPS format involves two distinct stages as shown in Algorithm 1: the construction of a CSR-part segment for the top r_{boundary} rows of the sparse matrix and the construction of a BCSR-part segment for the remaining rows.

Step 1: Constructing CSR-part. Given a standard CSR matrix (row_ptr , col_idx , vals), we extract the top r_{boundary} rows and form a CSR-part layout. This step involves copying relevant data from the original arrays, preserving the row structure. The new arrays $\text{row_ptr}'$, $\text{col_idx}'$, and vals' are updated accordingly to reflect the reduced row span.

Step 2: Constructing BCSR-part. For the remaining rows, we employ a tile-based layout. We define fixed tile dimensions (B_r, B_c) and iterate over each nonzero element to compute its corresponding tile location ($\text{tile_r}, \text{tile_c}$) and intra-tile offset. A hash map is maintained to record each unique tile’s address and to group the values accordingly.

3.3 Kernel design

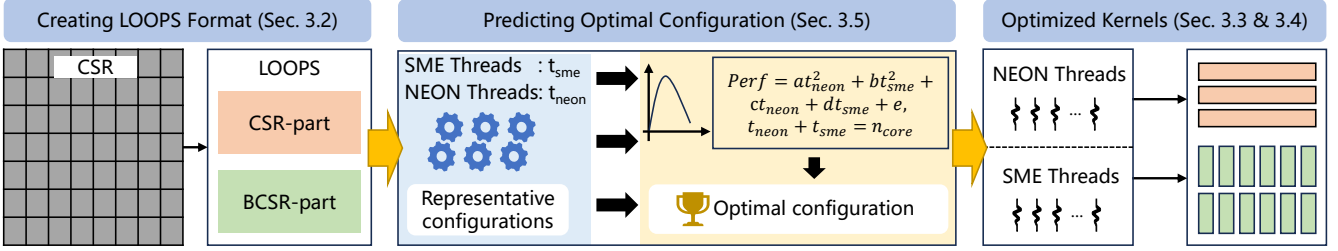


Figure 1. The overview of our SpMM pipeline.

Algorithm 1 Conversion from CSR to LOOPS Format

```

1: Input: CSR matrix row_ptr, col_idx, vals; row threshold r_boundary; row count row_end; tile size  $(B_r, B_c)$ 
2: Output: LOOPS format: CSR-part and BCSR-part
3: Initialize row_ptr', col_idx', vals'  $\leftarrow$  empty arrays
4: Initialize tile_map  $\leftarrow$  empty map
5: // Step 1: Build CSR-part
6: for  $i \leftarrow 0$  to  $r_{boundary} - 1$  do
7:   for  $k \leftarrow \text{row\_ptr}[i]$  to  $\text{row\_ptr}[i + 1] - 1$  do
8:     Append col_idx[k] to col_idx'
9:     Append vals[k] to vals'
10:  end for
11: Append current length of vals' to row_ptr'
12: end for
13: // Step 2: Build BCSR-part
14: for  $i \leftarrow r_{boundary}$  to  $r_{end} - 1$  do
15:   for  $k \leftarrow \text{row\_ptr}[i]$  to  $\text{row\_ptr}[i + 1] - 1$  do
16:      $j \leftarrow \text{col\_idx}[k]$ 
17:      $tile_r \leftarrow i \div B_r$ ,  $tile_c \leftarrow j \div B_c$ 
18:      $offset \leftarrow (i \bmod B_r) \cdot B_c + (j \bmod B_c)$ 
19:     if  $(tile_r, tile_c) \notin \text{tile\_map}$  then
20:        $\text{tile\_map}[(tile_r, tile_c)] \leftarrow$  new tile
21:     end if
22:      $\text{tile\_map}[(tile_r, tile_c)][offset] \leftarrow \text{vals}[k]$ 
23:   end for
24: end for

```

AXPY based NEON kernel for CSR part. For the CSR-part matrix A_{csr} , we design a NEON-optimized kernel that leverages row-wise sparsity and SIMD vectorization. The input sparse matrix is stored in a standard CSR layout, and the kernel performs row-wise accumulation by iterating over each nonzero element in the row of A and applying an AXPY operation with the corresponding row of matrix B . Specifically, for each nonzero element with column index j , we load the contiguous segments of B in row j into NEON registers and use fused multiply-add instructions to scale and accumulate these segments into the output row.

Outer-product based SME kernel for BCSR part. To preserve output locality and enhance cache efficiency, we do not compute the full outer product of an entire column of

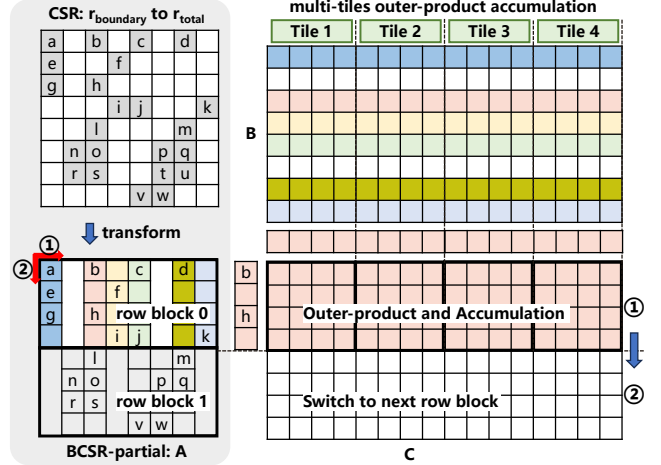


Figure 2. The BCSR-part SpMM workflow.

BCSR-part matrix A_{bcsr} and a full row of matrix B to form the partial result of the entire matrix C . Instead, the matrix A_{bcsr} is divided into a series of row blocks, each containing multiple rows of A_{bcsr} and further organized into a set of $B_r \times B_c$ -shaped tiles. Consider the FP64 case first. In our setting, we fix $B_r = \text{cntd}$ and $B_c = 1$, where cntd equals the maximum number of FP64 elements that a vector register can accommodate. The naive implementation of the FP64 SME-based BCSR-part SpMM is illustrated in Algorithm 2. The outermost loop (Line 4) iterates over all row blocks of matrix A_{bcsr} ; the second loop (Line 5) sweeps across the columns of matrix B in tiles of size cntd . These two loops together compute a $\text{cntd} \times \text{cntd}$ tile of the output matrix C . Lines 7–12 handle the loading of this output tile into a ZA tile register for accumulation. The core computation takes place in Lines 13–20, which iterate over all $\text{cntd} \times 1$ tiles within the current row block of A_{bcsr} , and the corresponding $1 \times \text{cntd}$ tiles in B . Each valid pair contributes to the outer-product update via SME instructions `fmopa`. Finally, Lines 21–26 store the accumulated result from the ZA tile back to memory. To further saturate the available ZA tile bandwidth and exploit the parallelism offered by the SME architecture, we implement a *multi-tile outer-product accumulation* strategy. As shown in Figure 2, instead of loading a single $1 \times \text{cntd}$ tile

Algorithm 2 BCSR-part SpMM with SME (FP64)

```

1: Input: BCSR matrix  $row\_ptr$ ,  $col\_idx$ ,  $vals$ ; row count
    $n_r$ ; row block count  $row_b$ ; tile count  $n_b$ ; tile row size  $B_r$ ;
   tile column size  $B_c$ ; N dim  $N$ ; dense matrix  $B$ 
2: Output: dense matrix  $C$ 
3:  $cntd \leftarrow \text{vector\_length} \div \text{sizeof}(double)$ 
4: for  $i \leftarrow 0$  to  $row_b$  do
5:   for  $j \leftarrow 0$  to  $N$  by  $cntd$  do
6:      $r_{begin} \leftarrow i \times B_r$ 
7:     for  $cnt \leftarrow 0$  to  $cntd$  do
8:       if  $cnt + r_{begin} \geq n_r$  then
9:         break
10:        end if
11:        load  $\&C[(r_{begin} + cnt) * N + j]$  to ZA tile
12:      end for
13:      for  $k \leftarrow row\_ptr[i]$  to  $row\_ptr[i + 1]$  do
14:         $col\_i \leftarrow col\_idx[k] \times B_c$ 
15:         $val\_offset \leftarrow k \times (B_r \times B_c)$ 
16:         $r_A \leftarrow vload(\&vals[val\_offset])$ 
17:         $r_B \leftarrow vload(\&B[col\_i \times N + j])$ 
18:        // Floating-point outer product and accumulate
19:         $fmopa(r_A, r_B)$ 
20:      end for
21:      for  $cnt \leftarrow 0$  to  $cntd$  do
22:        if  $cnt + r_{begin} \geq n_r$  then
23:          break
24:        end if
25:        store ZA tile to  $\&C[(r_{begin} + cnt) * N + j]$ 
26:      end for
27:    end for
28:  end for

```

of B at a time, we load multiple tiles of B simultaneously. This enables issuing multiple $fmopa$ instructions in parallel, each utilizing a different ZA tile. This optimization effectively increases the throughput of the innermost computation loop (Lines 13–20 in Algorithm 2).

For FP32, the only difference is that we fix $B_r = cntf$, where $cntf$ denotes the maximum number of FP32 elements that can be held in a single vector register. However, for FP16, since the f16f16f32 computation mode is the common precision setting in real-world applications and is supported by many vendor-provided libraries [4, 44], we reorganize the computation loops to align with the vectorized input-output format and accumulation constraints. Specifically, we utilize the FP16 sum of outer products and accumulate instruction which performs 2-way outer products accumulating the result in FP32 ZA tiles. As shown in Figure 3, this instruction takes two registers $h0$ and $h1$ of type FP16, each register holds $cnth$ FP16 elements. Then, the $cntf = cnth \div 2$ elements with indices $2i$ of $h0$ and $h1$ are widened to FP32 and an f32f32f32 outer-product is performed to obtain a $cntf \times cntf$ matrix $m0$. Similarly, the $cntf$ elements with indices $2i + 1$

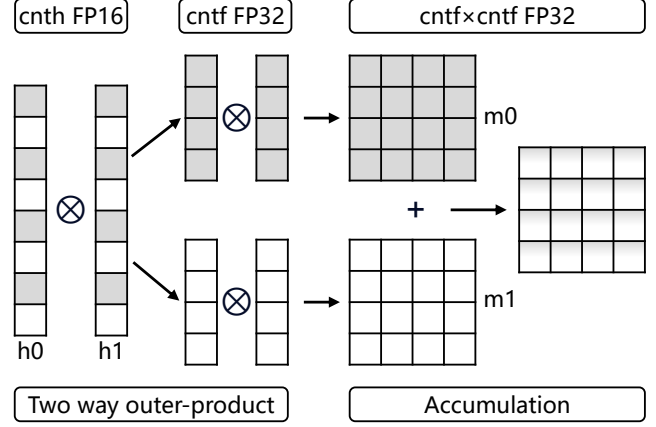


Figure 3. Illustration of FP16 two way fmopa instruction.

Algorithm 3 Core computation loop of BCSR-part SpMM with SME (FP16)

```

1: Input: BCSR matrix  $row\_ptr$ ,  $col\_idx$ ,  $vals$ ; row block
   index  $i$ ; block row size  $B_r$ ; block column size  $B_c$ ; N dim
    $N$ ; dense matrix  $B$ ; column index of  $B$   $j$ 
2: // Unroll the loop by 2 for two way outer-product.
3: for  $k \leftarrow row\_ptr[i]$  to  $row\_ptr[i + 1] - 1$  by 2 do
4:    $col\_i0 \leftarrow col\_idx[k] \times B_c$ 
5:    $col\_i1 \leftarrow col\_idx[k + 1] \times B_c$ 
6:    $val\_offset0 \leftarrow k \times (B_r \times B_c)$ 
7:    $val\_offset1 \leftarrow (k + 1) \times (B_r \times B_c)$ 
8:    $tmp0 \leftarrow vload(\&vals[val\_offset0])$ 
9:    $tmp1 \leftarrow vload(\&vals[val\_offset1])$ 
10:   $r0_A \leftarrow vzip1(tmp0, tmp1)$ 
11:   $r1_A \leftarrow vzip2(tmp0, tmp1)$ 
12:   $tmp0 \leftarrow vload(\&B[col\_i0 \times N + j])$ 
13:   $tmp1 \leftarrow vload(\&B[col\_i1 \times N + j])$ 
14:   $r0_B \leftarrow vzip1(tmp0, tmp1)$ 
15:   $r1_B \leftarrow vzip2(tmp0, tmp1)$ 
16:  // Four ZA tiles Floating-point outer product and ac-
   cumulate (widening, 2-way, FP16 to FP32)
17:   $fmopa(r0_A, r0_B)$ 
18:   $fmopa(r0_A, r1_B)$ 
19:   $fmopa(r1_A, r0_B)$ 
20:   $fmopa(r1_A, r1_B)$ 
21: end for
22: // A possible remaining tile is paired with the all-zero
   register and performs the same computation.

```

participate in an analogous operation to obtain a matrix $m1$ of the same size. Finally, $m0$ and $m1$ are element-wise accumulated to obtain the final FP32 result matrix. Leveraging this instruction, we design and implement the FP16 BCSR-part kernel in Algorithm 3. To accumulate the result to the appropriate place of result matrix C , we need to reorganize the elements within the vector register before computation.

Specifically, as shown in Algorithm 3, the loop in Line 3 processes two $cnth \times 1$ tiles (Lines 8–9) within the same row block. Then, Lines 10–11 employ the `vzip1` and `vzip2` instructions to perform register shuffling. Specifically, these instructions interleave the lower and higher halves of the loaded data, respectively, to form the correct order required for subsequent computation. For the possible remaining tile, we pair it with zero-filled vector register to ensure alignment and correctness of the computation pipeline.

3.4 Parallelization

To concurrently process the CSR-part and BCSR-part regions of the sparse matrix, we create two thread groups via OpenMP parallel sections to assign independent computation paths to different parts of the matrix. The first section handles the CSR part with a NEON kernel. Simultaneously, the second section processes the BCSR part using an SME kernel. This OpenMP-based division enables concurrent utilization of both NEON and SME execution pipelines, thereby maximizing throughput. Moreover, LOOPS is designed to facilitate thread-level parallelism without incurring synchronization overhead. Specifically, the CSR-part region is partitioned row-wise, and the BCSR-part region is partitioned row-block-wise, allowing independent threads to operate on disjoint subsets of rows or row blocks. Since each output row in the result matrix C is exclusively assigned to a single thread, inter-thread write conflicts are inherently avoided, eliminating the need for explicit atomics or locks. Furthermore, the number of threads for each parallel section can be tuned independently, allowing further flexibility in hardware resource allocation. This hybrid and hierarchical approach to parallelism, enabled by the LOOPS format, delivers both compute efficiency and scalability across NEON and SME units.

3.5 Adaptive scheduling for heterogeneous execution

3.5.1 Problem formulation. Modern CPUs often contain diverse execution units such as different SIMD extensions and dedicated co-processors, which use distinct pipelines. Therefore, to efficiently utilize these heterogeneous units, distributing workloads across them is critical to achieving high performance. Take M4Pro chip as an example. The scheduling problem is to determine the optimal thread partitioning between SME and NEON units for a given workload such that the predicted execution performance is maximized. Given a fixed total number of threads T , the search space consists of all $(t_{\text{neon}}, t_{\text{sme}})$ combinations satisfying $t_{\text{neon}} + t_{\text{sme}} \leq T$.

3.5.2 Performance prediction model. To model the performance impact of different thread partitions, we fit a polynomial regression model based on empirical measurements from a set of candidate configurations. The performance model is a quadratic function without cross terms since

NEON and SME execute in their dedicated pipelines:

$$\text{perf}(x, y) = a_0 + a_1x + a_2y + a_3x^2 + a_4y^2, \quad (2)$$

where x and y represent the number of threads assigned to NEON and SME units respectively, and $\text{perf}(x, y)$ is the predicted performance score. Coefficients (a_0, \dots, a_4) are computed using least squares fitting over the candidate set. The fitted model provides a lightweight analytical cost model to guide scheduling decisions at runtime.

3.5.3 Runtime scheduling strategy. At runtime, we enumerate all valid combinations of thread assignments that satisfy $t_{\text{neon}} + t_{\text{sme}} \leq T$, where T is the total number of cores. This enumeration is fast due to the limited core count. For each configuration, we compute the predicted performance using Equation (2), selecting the configuration with the highest predicted performance:

$$(t_{\text{neon}}^*, t_{\text{sme}}^*) = \arg \max_{x+y \leq T} \text{perf}(x, y). \quad (3)$$

This strategy enables the system to dynamically balance the compute workload across NEON and SME units, leveraging the strengths of both execution pipelines. Moreover, this scheduling mechanism is compatible with other adaptive techniques such as tiling and micro-kernel selection, and can be easily integrated into a larger auto-tuning framework.

4 Evaluation

4.1 Evaluation setup

Hardware platform. Experiments are conducted on an Apple Mac Mini equipped with the M4Pro chip. To the best of our knowledge, Apple M4Pro is the first publicly released commodity processor which adopts the Armv9 architecture. The chip features 12 CPU cores sharing two SME units. The system runs macOS 15.3.1 and all CPU codes are compiled using Clang 20.1.2 with `-O3`, `-fopenmp`, and `-march=armv9-a+sme+sve` options enabled. GPU experiments are conducted on a platform equipped with Intel Xeon Gold 6336Y (ICE-LAKE) CPU and NVIDIA A100-PCIE-40GB GPU. The system of the GPU platform runs Ubuntu 22.04.3 LTS and all the GPU methods compiled using `cuda-12.3 nvcc` (driver version 555.42.02) with the `-O3` and `-gencode arch=compute_80, code=sm_80` options on.

Baselines. We compare our LOOPS SpMM kernel with the following baselines:

- **TACO** [27]: A tensor algebra compiler that generates sparse code based on user-defined format and loop scheduling.
- **Armadillo** [41]: A high-level linear algebra library for C++ that provides sparse matrix support.
- **cuSparse** [35]: NVIDIA’s highly-optimized sparse linear algebra library.
- **Magicube** [30]: A state-of-the-art GPU SpMM approach that uses tiling and memory coalescing for high-throughput

Table 2. Representative matrices from the SuiteSparse Matrix Collection with feature values. *nrow* denotes the matrix row number. *NNZ* denotes the nonzero element number. *NNZ_x*, *NNZ_{mean}*, and *NNZ_{std}* denote the (maximum/minimum), mean, and standard deviation of the non-zero element number per row.

Id	Matrix	nrow	NNZ	NNZ _x	NNZ _{mean}	NNZ _{std}
m1	circuit5M	5.6M	59.5M	1.3M/1	10.71	1356.62
m2	Si41Ge41H72	0.2M	15.0M	662/13	80.86	126.97
m3	Ga41As41H72	0.3M	18.5M	702/18	68.96	105.39
m4	in-2004	1.4M	16.9M	7753/0	12.23	37.23
m5	eu-2005	0.9M	19.2M	6985/0	22.30	29.33
m6	pwtk	0.2M	11.6M	180/2	53.39	4.74
m7	FullChip	3.0M	26.6M	2.3M/1	8.91	1806.80
m8	mip1	0.1M	10.4M	66K/4	155.77	350.74
m9	mc2depi	0.5M	2.1M	4/2	3.99	0.08
m10	webbase-1M	1.0M	3.1M	4700/1	3.11	25.35
m11	shipsec1	0.1M	7.8M	102/24	55.46	11.07
m12	econ_fwd500	0.2M	1.3M	44/1	6.17	4.44
m13	scircuit	0.2M	1.0M	353/1	5.61	4.39
m14	pdb1HYS	0.0M	4.3M	204/18	119.31	31.86
m15	consph	0.1M	6.0M	81/1	72.13	19.08
m16	cant	0.1M	4.0M	78/1	64.17	14.06
m17	cop20k_A	0.1M	2.6M	81/0	21.65	13.79
m18	dc2	0.1M	0.8M	114K/1	6.56	361.50
m19	rma10	0.0M	2.4M	145/4	50.69	27.78
m20	ASIC_680k	0.7M	3.9M	395K/1	5.67	659.81

tensor core execution. We use their open-source implementation.

TACO and Armadillo are CPU codes evaluated under FP64 and FP32 precision settings; they do not support FP16. For the GPU codes, cuSparse is evaluated using all three precisions while Magicube only supports FP16. We fix $N = 32$ (the number of columns in dense matrix B) throughout all experiments, which reflects the common use case in deep learning and scientific kernels [16, 19, 26].

Datasets. We evaluate our method on the entire SuiteSparse Matrix Collection [12], comprising 4822 sparse matrices that span diverse domains and vary significantly in terms of size, sparsity pattern, and block density. This diversity ensures a comprehensive assessment of our method across representative sparse workloads. Meanwhile, we further select 20 matrices widely tested in previous work [33] in Table 2 to analyze the advantages of LOOPS in more detail. These group of sparse matrices come from multiple application domains and their scale ranges 0.8M to 59.5M non-zero values, and 36K to 5.6M rows.

Metrics. We report end-to-end SpMM compute throughput (in billions of floating-point operations, or GFLOPS), averaged over 1000 runs for each matrix. For the GPU codes, the host-device transfer time is excluded. For the CPU codes, only execution time is measured, excluding format transformation overhead.

4.2 Overall evaluation

Figure 4 depicts the GFLOPS performance of the CPU methods and cuSparse, ordered by increasing NNZ count (in log scale), in FP64 and FP32 precisions. Figure 5 illustrates the GFLOPS performance of LOOPS, cuSparse, and Magicube in FP16 precision (TACO and Armadillo are not included as they do not support FP16 precision). In addition, we present the speedup ratios of LOOPS relative to each baseline in Figure 6.

On the Apple M4Pro processor, LOOPS outperforms all CPU baselines across most matrices in all tested precisions. Specifically, compared to TACO, LOOPS delivers higher performance on 96.8% and 99.0% of the datasets, with an average speedup of 9.93 \times and 14.4 \times in FP64 and FP32 precisions, respectively. Furthermore, LOOPS outperforms Armadillo on 99.6% and 99.7% of the datasets, with an average speedup of 71.3 \times and 54.8 \times in FP64 and FP32 precisions, respectively. LOOPS also shows competitive performance with GPU baselines. Specifically, compared to cuSparse, LOOPS attains higher performance on 59.5%, 69.3%, and 75.8% of the datasets, with an average speedup of 21.8 \times , 28.3 \times , and 33.5 \times in FP64, FP32, and FP16 precisions, respectively. Finally LOOPS improves Magicube on 84.1% of the datasets, with an average speedup of 19.8 \times in FP16 precision.

Experimental results demonstrate that LOOPS achieves significantly higher throughput by effectively leveraging the matrix-level parallelism offered by SME and the vector-level capabilities of NEON. Compared to GPU approaches, LOOPS delivers superior performance when the NNZ is smaller than 10^6 , as GPU methods often suffer from under-utilization due to insufficient workload to saturate their compute and memory resources in those cases. For instance, LOOPS attains more than 30 \times speedup on matrices such as wheel_4_1, 1p_afiro, and the bibd_9_5 series, all of which contain fewer than 2000 non-zero entries. In contrast, for matrices with larger NNZ, GPU methods benefit from their massive parallelism, often achieving higher effective memory bandwidth and throughput. Nonetheless, the peak GFLOPS (the highest point in the scatter plot) is achieved by LOOPS, as shown in Figure 5. This advantage is primarily attributed to its sustained high compute throughput, particularly for matrices with high block density. For example, on the TSOPF_RS_b2383 matrix, where each block contains on average 25.10 non-zeros out of a maximum of 32, LOOPS achieves 1964.9 GFLOPS, substantially outperforming cuSparse (546.6 GFLOPS) and Magicube (336.9 GFLOPS).

Notably, the performance advantage of LOOPS becomes increasingly prominent at lower precisions, aligning with the design characteristics of SME, which provides significantly higher compute throughput for low-precision operations. Furthermore, for large matrices with regular sparsity patterns, LOOPS can achieve remarkably high performance that surpasses that of GPU methods, highlighting the advantage

of structured computation and effective hardware utilization on Armv9 CPUs.

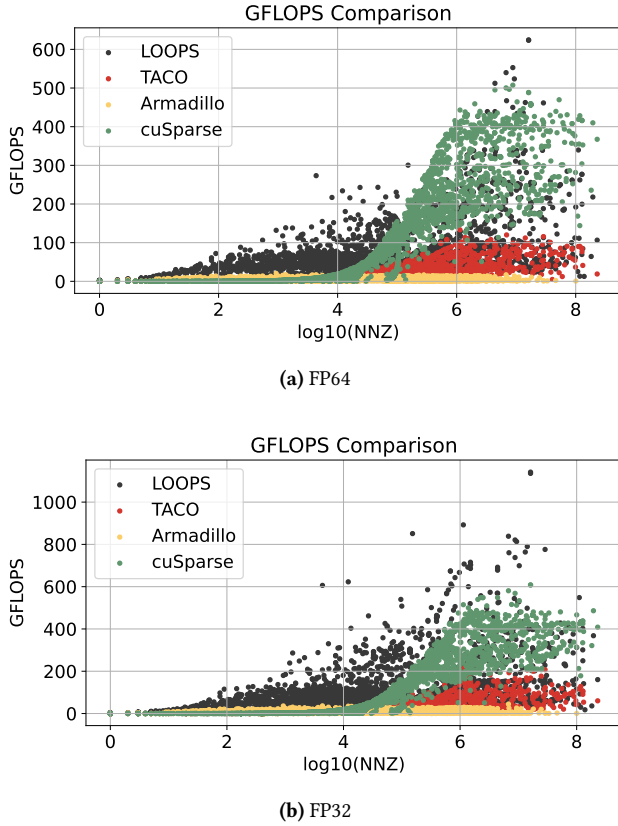


Figure 4. Overall SpMM performance (in GFLOPS) of CPU (on Apple M4Pro) and GPU SpMM methods (on NVIDIA A100) in (a) FP64 and (b) FP32 precisions.

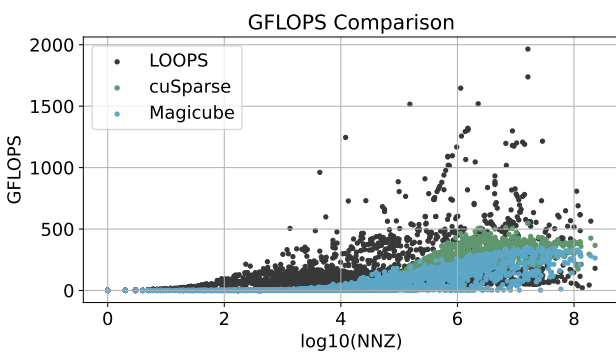


Figure 5. Overall SpMM performance (in GFLOPS) comparison of our method (on Apple M4Pro) with GPU SpMM methods (on NVIDIA A100) in FP16 precision.

4.3 Effectiveness of adaptive scheduling

We evaluate the effectiveness of our adaptive scheduling strategy in LOOPS by comparing it against two baselines: a pure NEON SpMM ($r_{boundary} = r_{total}$) implementation and a pure SME SpMM implementation ($r_{boundary} = 0$). The goal is to assess how well our approach leverages the NEON and SME units simultaneously. Experimental results on the entire SuiteSparse Matrix Collection demonstrate that LOOPS achieves the best performance on 83.3% of the matrices. On average, LOOPS delivers a 45.64 \times speedup over the pure NEON SpMM and a 124.72 \times speedup over the pure SME SpMM.

The substantial improvement over the SME-only baseline is primarily attributed to the inefficiency of multi-threaded SME execution for many matrices. Since SME resources are limited and shared across cores, aggressive parallel execution often leads to resource contention and degraded performance. In contrast, the adaptive scheduling of LOOPS dynamically selects single-threaded SME execution when appropriate, effectively avoiding contention and delivering superior performance for such workloads. The reason why LOOPS cannot deliver the best performance in some cases is that those matrices with extremely small row sizes, high sparsity irregularity, or very low computation-to-communication ratios tend to cause load imbalance or under-utilization of either NEON or SME units. Future work will enhance LOOPS to dynamically identify such corner cases at runtime and adapt the scheduling policies accordingly.

4.4 Energy efficiency

To evaluate the energy efficiency of our proposed method on Apple M4Pro, we compare the power consumption, runtime, and energy efficiency (GFLOPS/W) of LOOPS against cuSparse on NVIDIA A100 for 20 representative matrices in FP16 precision. The power consumption is measured by powermetrics tool and NVIDIA Management Library (NVML) [36] on Apple M4Pro and NVIDIA A100 respectively. It is worth noting that the number of the NNZ of all these 20 matrices exceeds 10^6 which can benefit from GPU execution more. As shown in Table 3, although the NVIDIA A100 achieves shorter runtime for most matrices due to its massive parallel throughput, it consumes significantly more power, averaging over 240W, compared to around 10–40W on Apple M4Pro. Interestingly, for several matrices such as m6, m8, and m14, and m17, LOOPS not only demonstrates lower power consumption but also achieves faster runtime than the cuSparse, resulting in up to 20 \times energy usage reduction. Overall, the results clearly indicate that LOOPS provides excellent energy efficiency. The benefits become more prominent in workloads with limited compute intensity, where high-end GPUs are often underutilized but still consume considerable power.

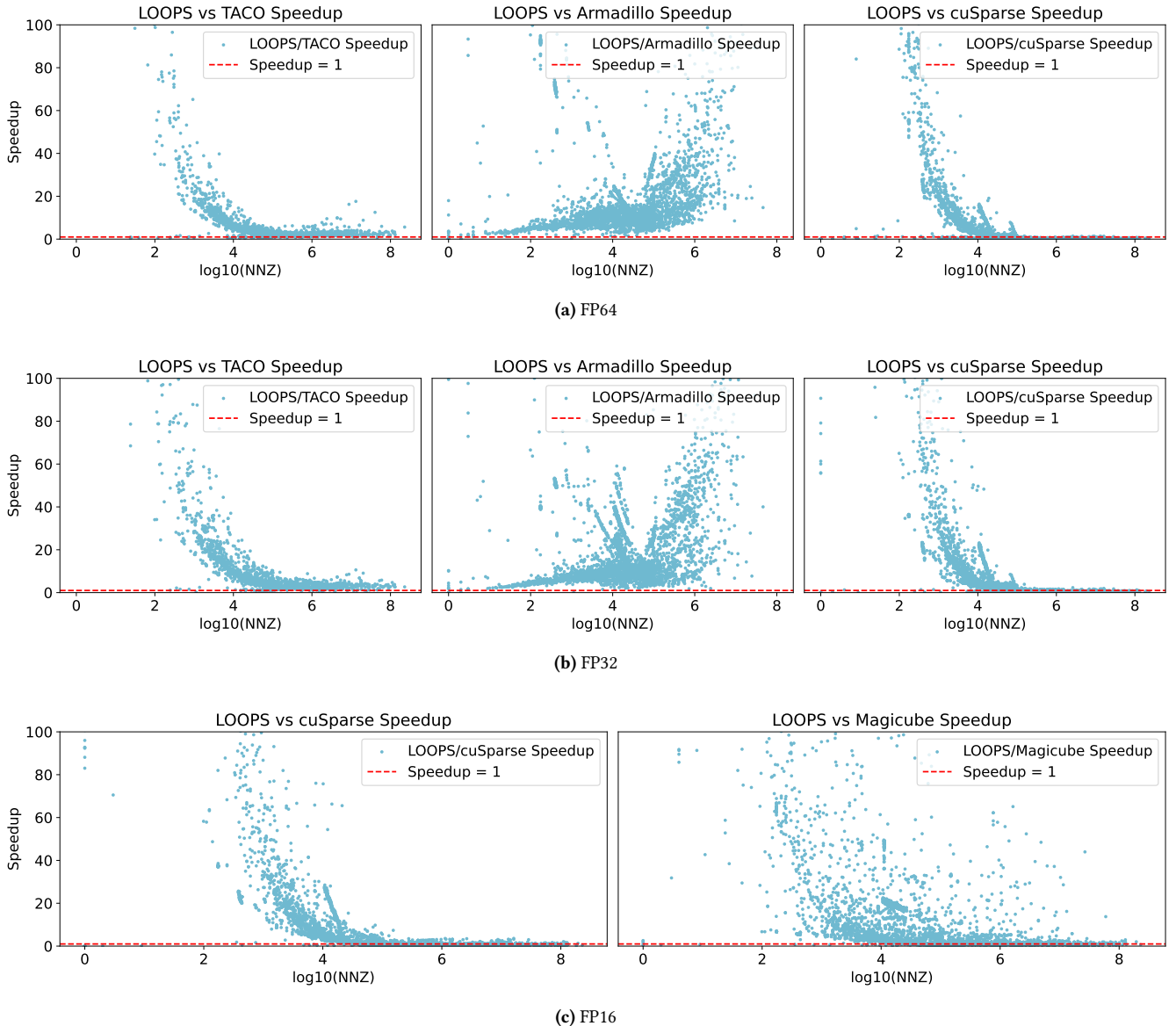


Figure 6. Performance speedup of our work, LOOPS, relative to the CPU- (TACO, Armadillo on Apple M4Pro) and GPU SpMM works (cuSparse, Magicube on NVIDIA A100) in (a) FP64, (b) FP32, and (c) FP16 precisions.

4.5 Case study: End-to-end GNNs performance

We integrate LOOPS into DGL [45] framework and choose a popular GNN model, specifically a Graph Convolutional Network (GCN) [20, 26] for end-to-end evaluation. GNN models mainly consist feature aggregation and feature update processes. For GCN, it aggregates features of neighbor nodes by the SpMM operator. As shown in Table 4, the graph datasets are selected from the built-in datasets of DGL, which is popular for evaluating the performance of GNNs. The end-to-end time includes the time of format conversion and model training. We select the latest DGL 2.5 with libxsmm [22] backend

enabled for performance comparison. Compared with DGL, LOOPS achieves speedups of 2.81 \times , 1.08 \times , and 1.12 \times for the three graphs. The difference in speedups is attributed to the block density. Under LOOPS format, the block density of Reddit dataset is 2.068, while the block density of Amazon-ratings dataset is only 1.028. This indicates that our method can bring more performance benefits when the nonzero entries of the dataset are more gathered. Meanwhile, the training accuracy of GCN using LOOPS kernel is consistent with the original DGL (no accuracy loss). Additionally,

Table 3. Power, time, and efficiency comparison between cuSparse on NVIDIA A100 and our method on Apple M4Pro for 20 matrices in FP16 precision.

Id	NVIDIA A100			Apple M4Pro		
	Power (W)	Time (s)	Eff. (GFLOPS/W)	Power (W)	Time (s)	Eff. (GFLOPS/W)
m1	247.8	0.8910	1.73	38.4	2.603	3.81
m2	245.8	0.1978	1.98	6.3	0.3678	41.46
m3	230.6	0.2770	1.85	36.9	0.5105	6.28
m4	247.4	0.1979	2.21	9.5	0.3771	30.22
m5	242.3	0.2667	1.91	10.2	0.4350	27.75
m6	247.3	0.1307	2.30	29.9	0.1079	23.08
m7	247.5	0.3967	1.74	31.0	1.190	4.62
m8	248.3	0.0929	2.87	12.3	0.0636	84.70
m9	235.9	0.0411	1.39	38.1	0.1136	3.11
m10	243.4	0.0599	1.36	37.8	0.1902	2.76
m11	242.2	0.0889	2.32	30.8	0.0985	16.48
m12	224.6	0.0233	1.56	41.8	0.1162	1.68
m13	211.4	0.0171	1.70	42.7	0.0562	2.56
m14	236.3	0.0438	2.69	10.2	0.0382	71.36
m15	247.2	0.0663	2.35	14.3	0.0744	36.16
m16	240.6	0.0440	2.42	17.7	0.0640	22.64
m17	96.5	0.2023	0.86	16.5	0.1194	8.53
m18	202.1	0.0133	1.82	33.6	0.0537	2.72
m19	236.2	0.0235	2.74	17.3	0.0431	20.38
m20	247.7	0.0675	0.89	8.4	0.1413	12.56

Table 4. Statistics of the evaluated datasets.

Dataset	Description	#Nodes	#Edges
Reddit	Reddit posts from September 2014	232,965	114,615,892
Amazon-ratings	Amazon co-purchasing network	24,492	186,100
Yelp	Yelp business network	716,847	13,954,819

for static GNN scenarios, preprocessing only needs to be performed once and can be easily amortized by multiple training epochs. Specifically, the preprocessing overhead accounts for only 1.3% of the end-to-end GNN training time.

5 Related Work

CPU SpMM. Optimized SpMM kernels on general-purpose CPUs remain relatively underexplored. Several existing efforts such as FusedMM [39], FeatGraph [24], and Rosko [34] focus on using SIMD instructions to accelerate SpMM. Additionally, vendor-provided libraries for CPUs, such as Intel MKL [44] or ArmPL [4], provide strong support for sparse linear algebra. However, ArmPL supports SpMV and SpGEMM, but does not support SpMM. Code-generation frameworks and auto-tuning systems such as TVM [9], LIBXSMM [22] and TACO [27] aim to generate optimized kernels for sparse workloads. However, they often struggle to adapt to rapidly evolving architectural features such as Armv9’s SME. For example, LIBXSMM currently provides SME support only for

dense GEMM kernels. Moreover, auto-tuning frameworks require significant search time and may introduce considerable tuning overhead.

GPU SpMM. Extensive work has been devoted to optimizing SpMM on GPUs. Sputnik [17] presents the one-dimensional tiling scheme and leveraging CUDA cores to accelerate sparse computation. vectorSparse [10] proposes the TCU-based 1-D Octet tiling method, using vectorized memory access. GE-SpMM [25] employs the warp merging strategy to reduce redundant data loading. To improve load balancing, RoDe [38] proposes a 2D strategy to divide the rows of sparse matrices into regular and residue parts and introduces new load balance and fine-grained pipeline technologies for further optimization. Current SOTA works typically use TCUs to push the SpMM performance to a new height. TC-GNN [46] and DTC-SpMM [15] propose custom sparse formats which divides the sparse matrix into nonzero vectors for computation on the TCUs. Magicube [30] is a high-performance sparse-matrix library to accelerate sparse and quantized matrix operations in deep learning leveraging the Strided Row-major BCRS (SR-BCRS) format. These approaches reconcile the sparse computation with the high-performance TCUs and employ multiple optimizations, including custom compressed format, reordering, load balancing, and pipeline optimizations.

DSA SpMM. Numerous domain-specific accelerators [18, 19, 21, 42] have been proposed to address the challenges of sparse computation. These accelerators primarily exploit sparsity patterns using customized memory hierarchies and compute units. For instance, Sextans [42] is a high performance FPGA accelerator for SpMM, which enables fast random access using on-chip memory, streaming access to off-chip large matrices, as well as PE-aware non-zero scheduling for balanced workload. SPADE [19] is a hardware accelerator for SpMM and SDDMM which avoids data transfer overheads by tightly coupling accelerator PEs with the cores of a multicore and attains flexibility and programmability by supporting a tile-oriented ISA. HotTiles [18] features heterogeneous SpMM accelerator architectures, which employ different types of PEs to exploit the insight that nonzeros form dense and sparse regions, rather than being uniformly distributed across the whole matrix. HYTE [31] is a hybrid static-dynamic framework to enable flexible and efficient tiling on sparse accelerators and can flexibly adapt to the specific data sparsity patterns. While such solutions demonstrate high performance and efficiency, they often lack flexibility and are not readily deployable on general-purpose processors.

Different from these works, LOOPS targets SME and NEON units on modern Arm architectures and introduces a hybrid sparse format and performance model to fully exploit the heterogeneity in compute resources. Additionally, LOOPS

achieves better (in small scale matrices) or comparable performance (in large scale matrices) against GPU methods with much lower power consumptions for SpMM on CPU.

6 Conclusion

In this paper, we propose LOOPS, a novel framework that integrates a hybrid sparse matrix format with a coordinated execution strategy to enable efficient collaboration between NEON and SME units on Armv9-based CPUs. LOOPS combines the CSR and BCSR layouts to map different portions of the workload to the distinct hardware execution units. Additionally, LOOPS supports multi-precision SpMM (FP64/FP32/FP16) and incorporates a lightweight performance model to guide dynamic scheduling decisions, achieving high performance and energy efficiency on the Apple M4Pro chip. Extensive experimental results show that LOOPS delivers state-of-the-art performance and energy efficiency for SpMM as well as end-to-end GNN performance.

References

- [1] Hasan Metin Aktulga, Aydin Buluç, Samuel Williams, and Chao Yang. 2014. Optimizing sparse matrix-multiple vectors multiplication for nuclear configuration interaction calculations. In *2014 IEEE 28th International Parallel and Distributed Processing Symposium*. IEEE, 1213–1222.
- [2] Hartwig Anzt, Stanimire Tomov, and Jack J Dongarra. 2015. Accelerating the LOBPCG method on GPUs using a blocked sparse matrix vector product. In *SpringSim (HPS)*. 75–82.
- [3] ARM. 2025. ARM Architecture Reference Manual. <https://developer.arm.com/documentation/ddi0487>.
- [4] ARM. 2025. ARM Performance Libraries 25.04. <https://developer.arm.com/documentation/109681/2504/Arm-Performance-Libraries-25-04-1-Release-Note>.
- [5] ARM. 2025. SME Programmer’s Guide. <https://developer.arm.com/documentation/109246>.
- [6] Manya Bansal, Olivia Hsu, Kunle Olukotun, and Fredrik Kjolstad. 2023. Mosaic: An interoperable compiler for tensor algebra. *Proceedings of the ACM on Programming Languages* 7, PLDI (2023), 394–419.
- [7] David M Blei, Andrew Y Ng, and Michael I Jordan. 2003. Latent dirichlet allocation. *Journal of machine Learning research* 3, Jan (2003), 993–1022.
- [8] Roberto L Castro, Andrei Ivanov, Diego Andrade, Tal Ben-Nun, Basilio B Fraguela, and Torsten Hoefer. 2023. Venom: A vectorized n: M format for unleashing the power of sparse tensor cores. In *Proceedings of the International Conference for High Performance Computing, Networking, Storage and Analysis*. 1–14.
- [9] Tianqi Chen, Thierry Moreau, Ziheng Jiang, Lianmin Zheng, Eddie Yan, Haichen Shen, Meghan Cowan, Leyuan Wang, Yuwei Hu, Luis Ceze, Carlos Guestrin, and Arvind Krishnamurthy. 2018. {TVM}: An automated {End-to-End} optimizing compiler for deep learning. In *13th USENIX Symposium on Operating Systems Design and Implementation (OSDI 18)*. 578–594.
- [10] Zhaodong Chen, Zheng Qu, Liu Liu, Yufei Ding, and Yuan Xie. 2021. Efficient tensor core-based gpu kernels for structured sparsity under reduced precision. In *Proceedings of the International Conference for High Performance Computing, Networking, Storage and Analysis*. 1–14.
- [11] Eli Chien, Jianhao Peng, Pan Li, and Olgica Milenkovic. 2020. Adaptive universal generalized pagerank graph neural network. *arXiv preprint arXiv:2006.07988* (2020).
- [12] Timothy A Davis and Yifan Hu. 2011. The University of Florida sparse matrix collection. *ACM Transactions on Mathematical Software (TOMS)* 38, 1 (2011), 1.
- [13] Adhitha Dias, Kirshanthan Sundararajah, Charitha Saumya, and Milind Kulkarni. 2022. SparseLNR: accelerating sparse tensor computations using loop nest restructuring. In *Proceedings of the 36th ACM International Conference on Supercomputing*. 1–14.
- [14] Erich Elsen, Marat Dukhan, Trevor Gale, and Karen Simonyan. 2020. Fast sparse convnets. In *Proceedings of the IEEE/CVF conference on computer vision and pattern recognition*. 14629–14638.
- [15] Ruibo Fan, Wei Wang, and Xiaowen Chu. 2024. Dtc-spmm: Bridging the gap in accelerating general sparse matrix multiplication with tensor cores. In *Proceedings of the 29th ACM International Conference on Architectural Support for Programming Languages and Operating Systems, Volume 3*. 253–267.
- [16] Qiang Fu, Thomas B Rolinger, and H Howie Huang. 2024. JITSPMM: Just-in-time instruction generation for accelerated sparse matrix-matrix multiplication. In *2024 IEEE/ACM International Symposium on Code Generation and Optimization (CGO)*. IEEE, 448–459.
- [17] Trevor Gale, Matei Zaharia, Cliff Young, and Erich Elsen. 2020. Sparse gpu kernels for deep learning. In *SC20: International Conference for High Performance Computing, Networking, Storage and Analysis*. IEEE, 1–14.
- [18] Gerasimos Gerogiannis, Sriram Aananthakrishnan, Josep Torrellas, and Ibrahim Hur. 2024. Hottiles: Accelerating spmm with heterogeneous accelerator architectures. In *2024 IEEE International Symposium on High-Performance Computer Architecture (HPCA)*. IEEE, 1012–1028.
- [19] Gerasimos Gerogiannis, Serif Yesil, Damitha Lenadora, Dingyuan Cao, Charith Mendis, and Josep Torrellas. 2023. Spade: A flexible and scalable accelerator for spmm and sddmm. In *Proceedings of the 50th Annual International Symposium on Computer Architecture*. 1–15.
- [20] Jaume Gibert, Ernest Valveny, and Horst Bunke. 2012. Graph embedding in vector spaces by node attribute statistics. *Pattern Recognition* 45, 9 (2012), 3072–3083.
- [21] Kartik Hegde, Hadi Asghari-Moghaddam, Michael Pellauer, Neal Crago, Aamer Jaleel, Edgar Solomonik, Joel Emer, and Christopher W Fletcher. 2019. Extensor: An accelerator for sparse tensor algebra. In *Proceedings of the 52nd Annual IEEE/ACM International Symposium on Microarchitecture*. 319–333.
- [22] Alexander Heinecke, Greg Henry, Maxwell Hutchinson, and Hans Pabst. 2016. LIBXSMM: accelerating small matrix multiplications by runtime code generation. In *SC’16: Proceedings of the International Conference for High Performance Computing, Networking, Storage and Analysis*. IEEE, 981–991.
- [23] Changwan Hong, Aravind Sukumaran-Rajam, Israt Nisa, Kunal Singh, and Ponnuswamy Sadayappan. 2019. Adaptive sparse tiling for sparse matrix multiplication. In *Proceedings of the 24th Symposium on Principles and Practice of Parallel Programming*. 300–314.
- [24] Yuwei Hu, Zihao Ye, Minjie Wang, Jiali Yu, Da Zheng, Mu Li, Zheng Zhang, Zhiru Zhang, and Yida Wang. 2020. Featgraph: A flexible and efficient backend for graph neural network systems. In *SC20: International Conference for High Performance Computing, Networking, Storage and Analysis*. IEEE, 1–13.
- [25] Guyue Huang, Guohao Dai, Yu Wang, and Huazhong Yang. 2020. Ge-spmm: General-purpose sparse matrix-matrix multiplication on gpus for graph neural networks. In *SC20: International Conference for High Performance Computing, Networking, Storage and Analysis*. IEEE, 1–12.
- [26] Thomas N Kipf and Max Welling. 2016. Semi-supervised classification with graph convolutional networks. *arXiv preprint arXiv:1609.02907* (2016).
- [27] Fredrik Kjolstad, Shoaib Kamil, Stephen Chou, David Lugato, and Saman Amarasinghe. 2017. The tensor algebra compiler. *Proceedings*

of the ACM on Programming Languages 1, OOPSLA (2017), 1–29.

[28] Andrew V Knyazev. 2001. Toward the optimal preconditioned eigensolver: Locally optimal block preconditioned conjugate gradient method. *SIAM journal on scientific computing* 23, 2 (2001), 517–541.

[29] Andrew S Lan, Andrew E Waters, Christoph Studer, and Richard G Baraniuk. 2014. Sparse factor analysis for learning and content analytics. *The Journal of Machine Learning Research* 15, 1 (2014), 1959–2008.

[30] Shigang Li, Kazuki Osawa, and Torsten Hoefer. 2022. Efficient quantized sparse matrix operations on tensor cores. In *SC22: International Conference for High Performance Computing, Networking, Storage and Analysis*. IEEE, 1–15.

[31] Xintong Li, Zhiyao Li, and Mingyu Gao. 2025. HYTE: Flexible Tiling for Sparse Accelerators via Hybrid Static-Dynamic Approaches. In *Proceedings of the 52nd Annual International Symposium on Computer Architecture*. 1613–1626.

[32] Baoyuan Liu, Min Wang, Hassan Foroosh, Marshall Tappen, and Marianna Pensky. 2015. Sparse convolutional neural networks. In *Proceedings of the IEEE conference on computer vision and pattern recognition*. 806–814.

[33] Yuechen Lu and Weifeng Liu. 2023. Dasp: Specific dense matrix multiply-accumulate units accelerated general sparse matrix-vector multiplication. In *Proceedings of the International Conference for High Performance Computing, Networking, Storage and Analysis*. 1–14.

[34] Vikas Natesh, Andrew Sabot, HT Kung, and Mark Ting. 2023. Rosko: Row Skipping Outer Products for Sparse Matrix Multiplication Kernels. *arXiv preprint arXiv:2307.03930* (2023).

[35] NVIDIA Corporation. 2025. cuSPARSE. <https://developer.nvidia.com/cusparse>.

[36] NVIDIA Corporation. 2025. NVIDIA Management Library (NVML). <https://developer.nvidia.com/management-library-nvml>.

[37] Patrik Okanovic, Grzegorz Kwasniewski, Paolo Sylos Labini, Maciej Besta, Flavio Vella, and Torsten Hoefer. 2024. High Performance Unstructured SpMM Computation Using Tensor Cores. In *SC24: International Conference for High Performance Computing, Networking, Storage and Analysis*. IEEE, 1–14.

[38] Meng Pang, Xiang Fei, Peng Qu, Youhui Zhang, and Zhaolin Li. 2024. A row decomposition-based approach for sparse matrix multiplication on GPUs. In *Proceedings of the 29th ACM SIGPLAN Annual Symposium on Principles and Practice of Parallel Programming*. 377–389.

[39] Md Khaledur Rahman, Majedul Haque Sujon, and Ariful Azad. 2021. Fusedmm: A unified sddmm-spmm kernel for graph embedding and graph neural networks. In *2021 IEEE International Parallel and Distributed Processing Symposium (IPDPS)*. IEEE, 256–266.

[40] Evann Regnault and Bérenger Bramas. 2023. SPC5: an efficient SpMV framework vectorized using ARM SVE and x86 AVX-512. *arXiv preprint arXiv:2307.14774* (2023).

[41] Conrad Sanderson and Ryan Curtin. 2016. Armadillo: a template-based C++ library for linear algebra. *Journal of Open Source Software* 1, 2 (2016), 26.

[42] Linghao Song, Yuze Chi, Atefeh Sohrabizadeh, Young-kyu Choi, Jason Lau, and Jason Cong. 2022. Sextans: A streaming accelerator for general-purpose sparse-matrix dense-matrix multiplication. In *Proceedings of the 2022 ACM/SIGDA International Symposium on Field-Programmable Gate Arrays*. 65–77.

[43] Petar Veličković, Guillem Cucurull, Arantxa Casanova, Adriana Romero, Pietro Lio, and Yoshua Bengio. 2017. Graph attention networks. *arXiv preprint arXiv:1710.10903* (2017).

[44] Endong Wang, Qing Zhang, Bo Shen, Guangyong Zhang, Xiaowei Lu, Qing Wu, and Yajuan Wang. 2014. Intel math kernel library. In *High-Performance Computing on the Intel® Xeon Phi™: How to Fully Exploit MIC Architectures*. Springer, 167–188.

[45] Minjie Wang, Da Zheng, Zihao Ye, Quan Gan, Mufei Li, Xiang Song, Jinjing Zhou, Chao Ma, Lingfan Yu, Yu Gai, Tianjun Xiao, Tong He, George Karypis, Jinyang Li, and Zheng Zhang. 2019. Deep graph library: A graph-centric, highly-performant package for graph neural networks. *arXiv preprint arXiv:1909.01315* (2019).

[46] Yuke Wang, Boyuan Feng, Zheng Wang, Guyue Huang, and Yufei Ding. 2023. {TC-GNN}: Bridging sparse {GNN} computation and dense tensor cores on {GPUs}. In *2023 USENIX Annual Technical Conference (USENIX ATC 23)*. 149–164.

[47] Kaige Zhang, Xiaoyan Liu, Hailong Yang, Tianyu Feng, Xinyu Yang, Yi Liu, Zhongzhi Luan, and Depei Qian. 2024. Jigsaw: Accelerating SpMM with Vector Sparsity on Sparse Tensor Core. In *Proceedings of the 53rd International Conference on Parallel Processing*. 1124–1134.

[48] Haisha Zhao, San Li, Jiaheng Wang, Chunbao Zhou, Jue Wang, Zhikuang Xin, Shunde Li, Zhiqiang Liang, Zhijie Pan, Fang Liu, Yan Zeng, Yangang Wang, and Xuebin Chi. 2025. Acc-SpMM: Accelerating General-purpose Sparse Matrix-Matrix Multiplication with GPU Tensor Cores. In *Proceedings of the 30th ACM SIGPLAN Annual Symposium on Principles and Practice of Parallel Programming*. 326–338.

[49] Jiang Zheng, Jiazhi Jiang, Jiangsu Du, Dan Huang, and Yutong Lu. 2023. Optimizing massively parallel sparse matrix computing on ARM many-core processor. *Parallel Comput.* 117 (2023), 103035.